Nonsymmetric evanescent coupling in photonics

Rodrigo A. Vicencio [1,2] Diego Román-Cortés [1,2] Martín Rubio-Saldías [1,2]
Paloma Vildoso [1,2] and Luis E. F. Foa Torres [1]

[1]*Departamento de Física, Facultad de Ciencias Físicas y Matemáticas, Universidad de Chile, Santiago 8370448, Chile*
[2]*Millenium Institute for Research in Optics-MIRO, Universidad de Chile, Chile*

Asymmetrical interactions are ubiquitous in nature, and in physics their study becomes fundamental. Despite the prevalence of evanescent coupling in physics, little attention has been paid to wave function profiles, with symmetrical reciprocal interactions often assumed for practical reasons. This work challenges that assumption by analytically demonstrating the origin of nonsymmetrical coupling in a photonic platform, focusing on the behavior of evanescent tails from adjacent waveguides. We experimentally validate an asymmetrical dynamics by studying detuned photonic directional couplers, fabricated via femtosecond laser writing, and corroborate our findings through continuous numerical simulations.

I. INTRODUCTION

A fundamental concept in lattice science is the study of localized wave functions bounded within well-defined spatial regions, such as waveguides or atoms. The tight-binding approximation [1] describes interactions between tightly bound orbitals at a given site that weakly interact with surrounding wave functions. This approach aims at examining the effects of weak coupling with neighboring sites. The approximation holds for well-separated sites where wave functions do not significantly overlap, as opposed to a strongly interacting regime [2,3]. In optics, analogous equations arise from coupled mode theory (CMT) [4], leading to key observations in transport and localization phenomena [5–9]. Here, the interwaveguide distance must exceed the waveguide widths to ensure minimal wave function distortion, allowing interactions between adjacent guided modes solely through evanescent fields. For more than two decades, research in photonic lattice phenomena [10–12] has predominantly assumed reciprocal coupling between waveguides. This assumption implies that the coupling constant between two waveguides is identical in both directions. Attempts to introduce nonreciprocity have mainly focused on simulating effective magnetic fields [9,13], which add a phase to the hopping terms but do not directly alter the wave function itself.

A nonreciprocal directional coupler (NRDC) was originally formulated long time ago in the context of resonant circuits [14]. Then, in the 1970s optical nonreciprocal devices started to be explored for integrated optics, and proposals for mode converters, isolators, and phase shifters were described [15]. Then, the validity of CMT was a main focus of research [16–19] looking for a better correspondence of the discrete model with exact numerical simulations. Some corrections to the simplest version of CMT were mandatory, with nonsymmetrical coupling constants being substantially different for nonidentical waveguides. At the end of the 1990s, magneto-optical waveguides were proposed for the construction of nonreciprocal Mach-Zehnder interferometers [20], and more

recently on-chip nonreciprocal optical resonators have been implemented in silicon [21]. Time modulation has been also suggested to implement nonreciprocity in compact integrated photonics, for example, using ringlike resonators or optomechanical cavities [22].

In this work, we demonstrate nonsymmetrical coupling interactions in photonic detuned dimers. We develop a standard formula for coupling coefficients considering steplike index waveguides, revealing the fundamental effect of evanescent profiles from neighboring waveguides. Our analysis shows that, opposite to the standard assumption, asymmetry is indeed an inherent property of photonic coupled systems, and it originates from the difference in refractive index profiles of two distant waveguides. Using the femtosecond (fs) laser writing technique [23], we fabricate photonic detuned couplers and experimentally demonstrate a nonsymmetrical dynamics. We corroborate all our observations through numerical simulations, without imposing any additional constraint but waveguide refractive index contrasts.

II. NONSYMMETRICAL PHOTONIC COUPLER MODEL

Let us start by studying a photonic coupler, such as the one sketched in Fig. 1(a), consisting of two waveguides separated a distance d. Coupled mode theory [24] generates different integrals which account for effective field interactions originated from the assumption that the total field is written as a linear combination of the modes at waveguides 1 and 2: $E_T = E_1 + E_2$. By assuming one-dimensional steplike index waveguides, we find different TE_{00} (transverse electric) modes, such as the ones sketched in Fig. 1(b), for the indicated refractive index contrasts Δn_i. In this case, mode profiles at the waveguide region (core) are proportional to $\cos(\alpha_i x)$, while outside (cladding) they decay as $\exp(-\gamma_i|x|)$. Fields are better confined (larger α, γ) for a growing Δn, and the neighbor field will be larger at the stronger waveguide [see Fig. 1(b) inset]. Therefore, we naturally expect to observe an asymmetric coupling interaction $C_{ij} \neq C_{ji}$ for inhomogeneous
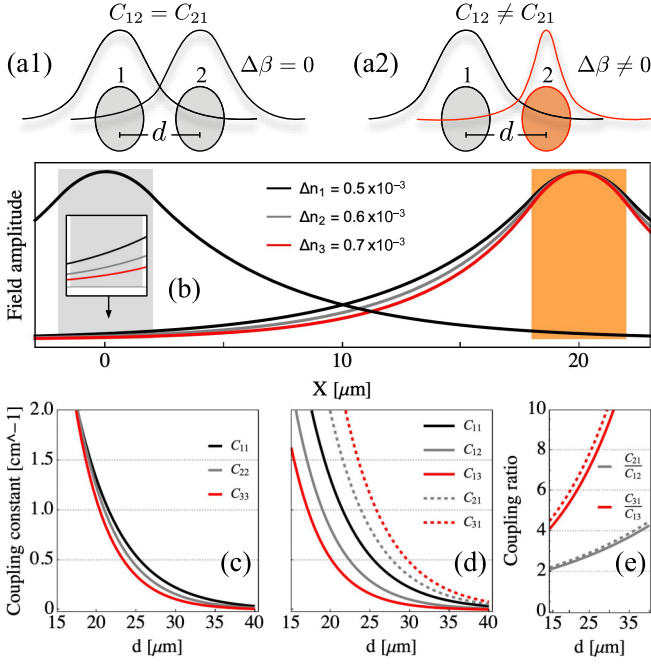
FIG. 1. (a1) Homogeneous and (a2) inhomogeneous photonic dimers. (b) Dimer configuration formed by steplike index waveguides. Fixed field amplitude at the left waveguide (Δn_1) and three different mode profiles at the right waveguide (Δn_1, Δn_2, and Δn_3). Coupling constant versus distance for (c) homogeneous and (d) inhomogeneous dimers. (e) Coupling ratio versus distance. Color code is indicated in (b).

couplers ($\Delta n_i \neq \Delta n_j$), with C_{ij} defined as [24]

$$C_{ij} = \omega\epsilon_0 \iint \left(n^2 - n_j^2\right)\vec{E}_j\vec{E}_i^* dx = \omega\epsilon_0 \Delta n_i^2 \int_i \vec{E}_j\vec{E}_i^* dx.$$

C_{ij} corresponds to a superposition integral at waveguide i, which measures the presence of mode E_i and the tail coming from a neighbor waveguide mode E_j (i and j are related to Δn_i and Δn_j, respectively).

First, we compute C_{ii} for homogeneous couplers for different refractive index contrasts and show the compiled results in Fig. 1(c). As expected, C_{ii} decreases as Δn_i increases. Now, we compute the coupling coefficients for inhomogeneous couplers, such as the one sketched in Fig. 1(a2). We immediately notice two strong effects that may define a *nonsymmetrical coupling interaction*. First, the mode asymmetry defines a larger coupling at the stronger waveguide, but also the coupling directly depends on the respective index contrast Δn_i. Therefore, *the asymmetry of coupling coefficients is not a weak effect and it cannot be neglected when considering detuned waveguides* [16]. We compute coupling coefficients with respect to a reference waveguide Δn_1 (black lines) and show the results in Fig. 1(d) (gray and red lines are related to Δn_2 and Δn_3, respectively). We notice that the coupling (C_{1j}) experienced by this reference waveguide decreases for an increasing contrast of the neighbor waveguide j. This is due to the fact that the neighbor mode tail becomes weaker and weaker in the reference waveguide region [see Fig. 1(b) inset]. On the other hand, when we ask the opposite question,

we find quite clearly that the coupling constant C_{j1} increases for an increasing contrast Δn_j.

We analytically compute a coupling constant ratio [25] to estimate the strength of this effect and show the results in Fig. 1(e). We observe a very strong asymmetry which grows quite fast with the separation distance d. We analytically approximate this ratio as

$$\frac{C_{ji}}{C_{ij}} \approx \left(\frac{\Delta n_j}{\Delta n_i}\right)^2 e^{(\gamma_j - \gamma_i)d}, \tag{1}$$

and plot it with dashed lines in Fig. 1(e). This expression states that two sites will experience a reciprocal and symmetric coupling interaction $C_{ij} = C_{ji}$ if and only if waveguides are equal or are able to balance this ratio. Coupling constants are the base of CMT for directional couplers [4], and almost all the results in lattice research have been developed under a symmetric assumption, which for example keeps the standard power and the Hamiltonian as conserved quantities [10].

However, Eq. (1) also gives a strong and fundamental physical result. For sites having different refractive index contrasts, which consequently support spatially different wave functions, we immediately notice that $C_{ij} \neq C_{ji}$. Therefore, nonsymmetrical coupling interactions emerge naturally in a photonic system. Specifically, if $\Delta n_1 < \Delta n_2$, the wave function at site 1 will be wider than the one at site 2 with $\gamma_1 < \gamma_2$ and, consequently, $C_{12} < C_{21}$. This is a counterintuitive result because strongly bounded wave functions (having a larger γ) will interact with a larger coupling coefficient. Our result is rather general and applies to any physical system experiencing an evanescent coupling interaction beyond optics and photonics.

Considering the previous analysis, a nonsymmetrical photonic coupler can be described by [24,25]

$$-i\frac{du_1}{dz} = \bar{\chi}_{21}u_1 + \bar{C}_{12}u_2 e^{-i\Delta\beta z},$$

$$-i\frac{du_2}{dz} = \bar{\chi}_{12}u_2 + \bar{C}_{21}u_1 e^{i\Delta\beta z}. \tag{2}$$

Here u_i describes the electric field mode amplitude at the ith site, z the propagation coordinate, $\Delta\beta \equiv \beta_2 - \beta_1$ defines the propagation constants' detuning,

$$\bar{\chi}_{ij} \equiv \frac{\chi_{ij} - C_{ij}N_{ij}}{1 - |N_{ij}|^2},$$

and

$$\bar{C}_{ij} \equiv \frac{C_{ij} - \chi_{ij}N_{ij}}{1 - |N_{ij}|^2}.$$

Coefficient $\bar{\chi}_{ij}$ is also nonsymmetric and depends on the integral χ_{ij}, defined as

$$\chi_{ij} = \omega\epsilon_0 \Delta n_i^2 \iint_i |\vec{E}_j|^2 dx\,dy,$$

which describes the presence of the field j at waveguide i (see more details in [25]). $\bar{C}_{12}$ and $\bar{C}_{21}$ correspond to modified coupling constants or, simply, coupling terms. Integral $N_{12} = N_{21}$ expresses a nonorthogonal contribution for the superposition of modes coming from different waveguides [17,26], and it
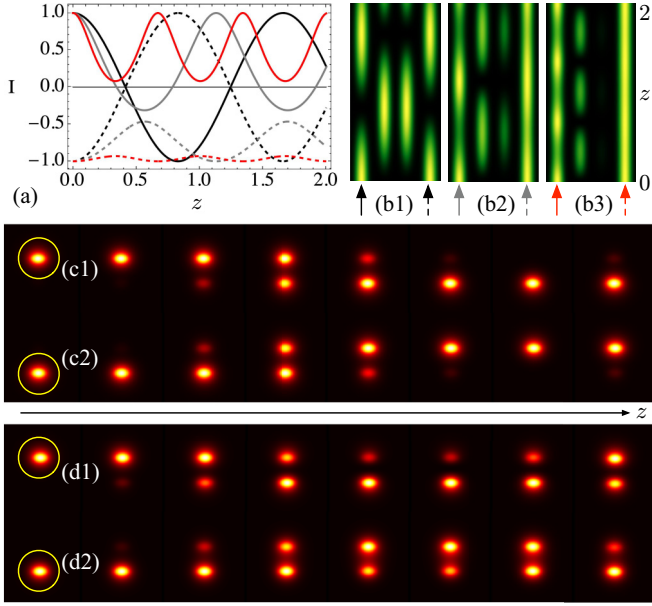
FIG. 2. (a) Imbalance dynamics from model (2) for the excitation of the first (full line) and second (dashed line) waveguides for $\Delta n_1 - \Delta n_1$ (black), $\Delta n_1 - \Delta n_2$ (gray), and $\Delta n_1 - \Delta n_3$ (red) configurations. (b) Normalized power evolution, with arrows indicating the input positions and respective case relative to (a). (c) and (d) Intensity profiles versus z, obtained from continuous simulations, after exciting the (c1), (d1) first and the (c2), (d2) second waveguides. $d = 18$ μm.

can be written as

$$N_{ij} = \frac{1}{\omega\mu_0}(\beta_i + \beta_j) \int_{-\infty}^{\infty} E_j E_i^* \, dx,$$

for the steplike index TE_{00} case. The normalization condition $N_{ii} = 1$ is imposed in this derivation, and we find that $N_{12} < 0.3 \ll 1$ [25] and, therefore, in practice

$$\bar{\chi}_{ij} \approx \chi_{ij} \quad \text{and} \quad \bar{C}_{ij} \approx C_{ij}.$$

Model (2) describes a completely general dimer model including effective site detuning and nonsymmetrical coupling. Although model (2) is non-Hermitian, the eigenvalues are real and are given by

$$\bar{\lambda}_{\pm} = \pm\bar{\lambda}_0 = \pm\sqrt{(\Delta\beta + \bar{\chi}_{21} - \bar{\chi}_{12})^2/4 + \bar{C}_{12}\bar{C}_{21}}.$$

A standard power definition [10] is not a conserved quantity of model (2), but the *nonsymmetric power* $P_r \equiv P_1 + \bar{C}_{12}P_2/\bar{C}_{21}$ is, with $P_i = |u_i|^2$. The excitation of waveguide i generates a power evolution

$$P_i^i(z) = \cos^2(\lambda_0 z) + (\Delta\beta/2\lambda_0)^2 \sin^2(\lambda_0 z)$$

for the excited waveguide, and

$$P_j^i(z) = (\bar{C}_{ji}/\bar{\lambda}_0)^2 \sin^2(\bar{\lambda}_0 z)$$

for the nonexcited waveguide j ($i \neq j$) [25]. Using this, we obtain a coupling ratio from dynamics given by

$$\frac{P_2^1(z)}{P_1^2(z)} = \left(\frac{\bar{C}_{21}}{\bar{C}_{12}}\right)^2 \approx \left(\frac{C_{21}}{C_{12}}\right)^2. \tag{3}$$

Therefore, depending on the excited site, asymmetry on coupling terms immediately produces an asymmetric dynamics. Specifically, for $C_{21} > C_{12}$ the exchange of energy will be more efficient when exciting waveguide 1, as we will show below.

In order to study the effect of this asymmetry in the dynamics, we define the *imbalance* as

$$I_i = \left(P_1^i - P_2^i\right)/\left(P_1^i + P_2^i\right).$$

For a reciprocal-symmetrical system the imbalance must be symmetric and the excitation of the first or the second waveguides should show mirror-symmetric curves only, independently of detuning [27]. We first explore a symmetric-reciprocal dimer, such as the one shown in Fig. 1(a1), with the two waveguides having a contrast Δn_1. Results are shown in Figs. 2(a) (black) and 2(b1) for $\bar{C}_{12} = \bar{C}_{21} = 1.89$ cm^{-1}, $\bar{\chi}_{12} = \bar{\chi}_{21} = -0.24$ cm^{-1}, and $\Delta\beta = 0$. We observe a fully symmetric energy exchange, as expected for a reciprocal directional coupler [4,24]. Then, we asymmetrize the system [see sketch in Fig. 1(a2)] by taking a second waveguide with Δn_2, such that $\bar{\chi}_{21}/\bar{\chi}_{12} = 2.02$, $\bar{C}_{21}/\bar{C}_{12} = 2.28$, and $\Delta\beta = 4.24$ cm^{-1}. In this case the dynamics [see Figs. 2(a) (gray) and 2(b2)] expresses a small asymmetry. We observe how the excitation of the first waveguide crosses the symmetrical point $I = 0$ (i.e., a 50/50 beam splitter) but it is not able to transfer all the power into the second waveguide. Alone, this is not a signature of nonsymmetrical dynamics. But, in addition, we observe that the excitation of the second waveguide does not follow a mirror-reflected trajectory and, in fact, it is not able to even reach the symmetrical point [see Fig. 2(a), dashed gray line]. Both considerations define a nonsymmetrical dimer. A stronger nonsymmetrical case is shown in Figs. 2(a) (red) and 2(b3) with $\bar{\chi}_{21}/\bar{\chi}_{12} = 3.54$, $\bar{C}_{21}/\bar{C}_{12} = 4.85$, and $\Delta\beta = 8.86$ cm^{-1}. We observe that the excitation of the first (softer) waveguide shows a close-to-zero imbalance, while the excitation of the second (stronger) site shows an almost null transfer. These examples show that the observation of a Hadamard regime ($\Delta\beta = 2C_{12} = 2C_{21}$) [28–30] is indeed not possible on a nonsymmetrical coupler, due to the inherent asymmetry of this system.

We check model (2) by means of a continuous approach [25] and an *Eigenmode expansion method*. As the dynamics is governed by an initial projection on linear modes, the computation of them allows us to obtain the evolution of the electric field along the propagation coordinate z. Figures 2(c) and 2(d) show examples of the obtained dynamics for a symmetric ($\Delta n_a - \Delta n_a$) and a nonsymmetric ($\Delta n_a - \Delta n_b$) configuration, respectively, for $\Delta n_a = 0.4 \times 10^{-3}$ and $\Delta n_b = 0.44 \times 10^{-3}$. We observe that an homogeneous and reciprocal coupler follows a standard symmetric oscillation, with an opposite imbalance [25]. On the other hand, an inhomogeneous coupler shows an asymmetric dynamics where the excitation of the softer waveguide [Fig. 2(d1)] produces a larger energy transfer compared to the excitation of the stronger site [Fig. 2(d2)]. Simulations in Figs. 2(c) and 2(d) were performed without any constraint but with a definition of waveguides having a given refractive index contrast.
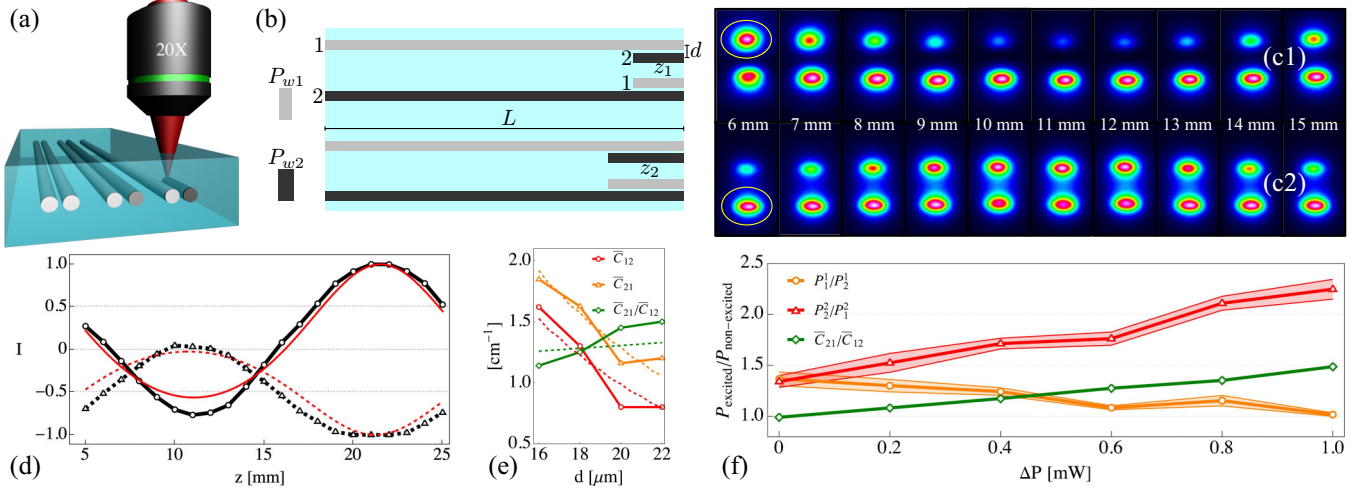
FIG. 3. (a) Sketch of the femtosecond laser writing technique. (b) z-scan method for detuned couplers, fabricated with powers P_1 (gray stripes) and P_2 (black stripes), for a propagation distance z_i. Output intensity images versus z_i for the excitation of the (c1) top and (c2) bottom waveguides, for $d = 18$ μm. (d) Experimental extracted imbalance versus $z_i \in \{5, 25\}$ mm for (c1), black full line, and (c2), black dashed line. Red lines in (d) correspond to a model (2) prediction. (e) Experimentally obtained couplings $\bar{C}_{12}$, $\bar{C}_{21}$ and ratio $\bar{C}_{21}/\bar{C}_{12}$ versus distance d, for $\Delta P = 1$ mW. Dashed lines in (e) show results from continuous simulations. (f) Average power ratio P_i^i/P_j^i and its standard deviation versus ΔP. Orange and red data correspond to the excitation of waveguides 1 and 2, respectively. Green data shows the extracted nonsymmetric coupling ratio according to (3).

III. EXPERIMENTAL OBSERVATION OF NONSYMMETRICAL DYNAMICS

Now, we provide experimental evidence for nonsymmetrical coupling interactions. We fabricate several detuned photonic dimers using the fs laser writing technique [23] on a borosilicate glass wafer, as sketched in Fig. 3(a). A way to achieve detuned waveguides is by directly varying the fabrication parameters; i.e., laser power and/or writing velocity. The larger the power and the slower the velocity, the stronger the refractive index change [23,27]. We set the velocity to $v = 2.5$ mm/s and the writing power P_{w1} for waveguide 1. Nonsymmetric couplers are fabricated by applying a larger writing power P_{w2} for waveguide 2. In all the experiments, we collect intensity images with a beam profiler at the output facet of a $L = 30$ mm long wafer. The dynamics along the z coordinate can be studied by conducting a z-scan experiment [27]: dimers are fabricated in pairs with a full waveguide of length L plus a shorter waveguide of length z_i, separated by an intersite distance d, as sketched in Fig. 3(b), such that we can excite the first and second waveguides of an equivalent coupler.

The z-scan experiment runs in the interval $z_i \in \{5, 25\}$ mm, every 1 mm, and we show a shorter set of images in Fig. 3(c). In this case, bottom waveguides were fabricated such that $\Delta P \equiv P_{w2} - P_{w1} = 5$ mW, for $d = 18$ μm. Figure 3(c1) shows an out-of-phase dynamical evolution after exciting waveguide 1, where we observe an almost full energy transfer at $z \approx 11$ mm [$I \sim -0.75$ in Fig. 3(d)]. On the other hand, ~50% of the energy is transferred by exciting waveguide 2 as shown in Fig. 3(c2), with $I \sim 0$ in Fig. 3(d). The images shown in Fig. 3(c), and the compiled imbalance data of Fig. 3(d) (black), give a clear experimental proof of nonsymmetrical dynamics, with asymmetric trajectories after initializing the system at opposite waveguides. We

perform a calibration of parameters by fitting analytical dimer solutions [16,25] from model (2) with the data shown in Fig. 3(c). Results are shown with red lines in Fig. 3(d), for $\Delta\beta + \bar{\chi}_{21} - \bar{\chi}_{12} \approx 1.8$ cm^{-1}, $\bar{C}_{12} \approx 0.85$ cm^{-1}, and $\bar{C}_{21} \approx 1.70$ cm^{-1}. This example shows an indeed strong asymmetry with a coupling ratio $\bar{C}_{21}/\bar{C}_{12} \approx 2.0$.

We implement several experiments to confirm this very fundamental observation. For example, we set a smaller power detuning $\Delta P = 1$ mW and fabricate several couplers for different intersite distances d, including a z-scan experiment to extract the coupling parameters. Figure 3(e) shows our compiled results for coupling constants, where we observe a standard decreasing dependence [23,27]. We also notice a clear gap in between $\bar{C}_{12}$ and $\bar{C}_{21}$, confirming the nonsymmetrical nature of the detuned photonic couplers. We compute the ratio $\bar{C}_{21}/\bar{C}_{12}$ (see green full line) and observe an increasing tendency while increasing the intersite distance, in agreement with prediction (1). In addition, we confirm these experimental findings by continuous numerical simulations [see dashed lines in Fig. 3(e)], assuming detuned couplers with a small refractive index difference $\Delta n \equiv n_2 - n_1 = 0.2 \times 10^{-4}$.

Finally, we confirmed statistically the observed nonsymmetrical dynamics by repeating the dimer experiments several times, for a fixed set of parameters: P_{w1}, $d = 20$ μm, and $z_1 = 6$ mm. We fabricate a set couplers pairs, where the long and short waveguides are simply exchanged [see Fig. 3(b)]. We fabricate the clone systems ten times and obtain a rough statistical confirmation for different detuned waveguides with an increasing power detuning ΔP. Our compiled results are shown in Fig. 3(f). As nonsymmetrical interactions are dynamically evidenced by an asymmetric evolution, in this experiment we measured the output power ratio among the excited and the nonexcited waveguides: P_i^i/P_j^i. Figure 3(f) shows our averaged results, where we clearly observe a

nonsymmetrical dynamics, with a very small standard deviation. Only for equal waveguides ($\Delta P = 0$) we observe a convergent dynamics with an equal power ratio, as expected for homogeneous coupler systems. However, once ΔP increases, we start observing a divergent dynamics: the excitation of the low power waveguide (P_{w1}) produces a larger energy transfer (smaller ratio), while the excitation of the higher power waveguide (P_{w2}) tends to keep the energy trapped at the input site (larger ratio). From (3) we compute the ratio in between both experiments and obtain a coupling ratio $\bar{C}_{21}/\bar{C}_{12}$ [see green data in Fig. 3(f)], which increases linearly with the writing power ΔP (detuning).

IV. CONCLUSIONS

In this work, we have developed the concept of nonsymmetrical coupling emerging from detuned photonic waveguides. We analytically, numerically, and experimentally demonstrated that detuned mode profiles lead to nonsymmetric coupling constants. While evanescent coupling is a natural phenomenon in optics, we believe this concept could be extended to other physical contexts with similar descriptions based on superposition integrals. All experimental observations were corroborated by extensive numerical simulations of a paraxial wave equation, using only realistic optical parameters without additional constraints. Our findings demonstrate that standard table-top experiments can now be used to study more complex phenomena, potentially opening new research directions and having a broad impact in physics, and science in general. Breaking the symmetry is fundamental yet challenging to achieve in compact integrated devices [22], and our proposal offers a clear and simple solution to this fundamental challenge in applied photonics [28–32] with, in principle, a small footprint and scalability. Our experimental proposal could be extended to non-Hermitian systems [33–38], where different exotic transport properties emerge [39–41].

[1] C. Kittel, *Introduction to Solid State Physics*, 8th ed. (Wiley, Hoboken, NJ, 2005).

[2] E. Kaxiras, *Atomic and Electronic Structure of Solids* (Cambridge University Press, Cambridge, 2003).

[3] M. Mazanov, D. Román-Cortés, G. Cáceres-Aravena, C. Cid, M. A. Gorlach, and R. A. Vicencio, Nano Lett. **24**, 4595 (2024).

[4] A. Yariv and P. Yeh, *Optical Waves in Crystals: Propagation and Control of Laser Radiation*, Wiley Classics Library ed. (John Wiley and Sons, Hoboken, NJ, 2003).

[5] R. Morandotti, U. Peschel, J. S. Aitchison, H. S. Eisenberg, and Y. Silberberg, Phys. Rev. Lett. **83**, 4756 (1999).

[6] T. Schwartz, G. Bartal, S. Fishman, and M. Segev, Nature (London) **446**, 52 (2007).

[7] C. E. Rüter, K. G. Makris, R. El-Ganainy, D. N. Christodoulides, M. Segev, and D. Kip, Nat. Phys. **6**, 192 (2010).

[8] R. A. Vicencio, C. Cantillano, L. Morales-Inostroza, B. Real, C. Mejía-Cortés, S. Weimann, A. Szameit, and M. I. Molina, Phys. Rev. Lett. **114**, 245503 (2015).

[9] M. C. Rechtsman, J. M. Zeuner, Y. Plotnik, Y. Lumer, D. Podolsky, F. Dreisow, S. Nolte, M. Segev, and A. Szameit, Nature (London) **496**, 196 (2013).

[10] F. Lederer, G. I. Stegeman, D. N. Christodoulides, G. Assanto, M. Segev, and Y. Silberberg, Phys. Rep. **463**, 1 (2008).

[11] T. Ozawa, H. M. Price, A. Amo, N. Goldman, M. Hafezi, L. Lu, M. C. Rechtsman, D. Schuster, J. Simon, O. Zilberberg, and I. Carusotto, Rev. Mod. Phys. **91**, 015006 (2019).

[12] R. A. Vicencio Poblete, Adv. Phys. X **6**, 1878057 (2021).

[13] S. Mukherjee, M. Di Liberto, P. Öhberg, R. R. Thomson, and N. Goldman, Phys. Rev. Lett. **121**, 075502 (2018).

[14] H. Berger, IEEE Trans. Microwave Theory Tech. **13**, 474 (1965).

[15] S. Yamamoto and T. Makimoto, J. Appl. Phys. **45**, 882 (1974).

[16] A. Hardy and W. Streifer, J. Lightwave Technol. **3**, 1135 (1985).

[17] H. Haus, W. Huang, S. Kawakami, and N. Whitaker, J. Lightwave Technol. **5**, 16 (1987).

[18] E. A. J. Marcatili, L. L. Buhl, and R. C. Alferness, Appl. Phys. Lett. **49**, 1692 (1986).

[19] W.-P. Huang, J. Opt. Soc. Am. A **11**, 963 (1994).

[20] N. Bahlmann, M. Lohmeyer, O. Zhuromskyy, H. Dötsch, and P. Hertel, Opt. Commun. **161**, 330 (1999).

[21] L. Bi, J. Hu, P. Jiang, D. H. Kim, G. F. Dionne, L. C. Kimerling, and C. A. Ross, Nat. Photonics **5**, 758 (2011).

[22] D. L. Sounas and A. Alù, Nat. Photonics **11**, 774 (2017).

[23] A. Szameit, D. Blömer, J. Burghoff, T. Schreiber, T. Pertsch, S. Nolte, A. Tünnermann, and F. Lederer, Opt. Express **13**, 10552 (2005).

[24] *Fundamentals of Optical Waveguides*, K. Okamoto, 3rd ed. (Academic, New York, 2022), pp. 159–166.

[25] See Supplemental Material at http://link.aps.org/supplemental/10.1103/PhysRevA.111.043510 for formal derivation of equations, integral estimations, analytical solutions, continuous numerical simulations, experimental setup, and experimental data.

[26] J. Schulz, C. Jörg, and G. von Freymann, Opt. Express **30**, 9869 (2022).

[27] D. Guzmán-Silva, G. Cáceres-Aravena, and R. A. Vicencio, Phys. Rev. Lett. **127**, 066601 (2021).

[28] E. Polino, M. Riva, M. Valeri, R. Silvestri, G. Corrielli, A. Crespi, N. Spagnolo, R. Osellame, and F. Sciarrino, Optica **6**, 288 (2019).

[29] G. Moody, V. J. Sorger, D. J. Blumenthal, P. W. Juodawlkis, W. Loh, C. Sorace-Agaskar, A. E. Jones, K. C. Balram, J. C. F. Matthews, A. Laing, M. Davanco, L. Chang, J. E. Bowers, N.

Quack, C. Galland, I. Aharonovich, M. A. Wolff, C. Schuck, N. Sinclair, M. Lončar *et al.* J. Phys. Photonics **4**, 012501 (2022).

[30] T. Meany, M. Gräfe, R. Heilmann, A. Perez-Leija, S. Gross, M. J. Steel, M. J. Withford, and A. Szameit, Laser Photonics Rev. **9**, 363 (2015).

[31] Y.-J. Chang, Y.-H. Lu, Y. Wang, X.-Y. Xu, W.-H. Zhou, W.-H. Cui, X.-W. Wang, J. Gao, L.-F. Qiao, and X.-M. Jin, Phys. Rev. Lett. **126**, 110501 (2021).

[32] A. Politi, M. J. Cryan, J. G. Rarity, S. Yu, and J. L. O'Brien, Science **320**, 646 (2008).

[33] V. M. Martinez Alvarez, J. E. Barrios Vargas, and L. E. F. Foa Torres, Phys. Rev. B **97**, 121401(R) (2018).

[34] L. E. F. Foa Torres, J. Phys. Mater. **3**, 014002 (2020).

[35] E. J. Bergholtz, J. C. Budich, and F. K. Kunst, Rev. Mod. Phys. **93**, 015005 (2021).

[36] S. Yao and Z. Wang, Phys. Rev. Lett. **121**, 086803 (2018).

[37] R. Lin, T. Tai, L. Li, and C. H. Lee, Front. Phys. **18**, 53605 (2023).

[38] N. Okuma and M. Sato, Annu. Rev. Condens. Matter Phys. **14**, 83 (2023).

[39] Y. G. N. Liu, Y. Wei, O. Hemmatyar, G. G. Pyrialakos, P. S. Jung, D. N. Christodoulides, and M. Khajavikhan, Light: Sci. Appl. **11**, 336 (2022).

[40] S. Weidemann, M. Kremer, T. Helbig, T. Hofmann, A. Stegmaier, M. Greiter, R. Thomale, and A. Szameit, Science **368**, 311 (2020).

[41] T. Helbig, T. Hofmann, S. Imhof, M. Abdelghany, T. Kiessling, L. W. Molenkamp, C. H. Lee, A. Szameit, M. Greiter, and R. Thomale, Nat. Phys. **16**, 747 (2020).